Virology | Full-Length Text

Human coronavirus OC43 infection remodels connexin 43-mediated gap junction intercellular communication *in vitro*

Souvik Karmakar,[1] Jayasri Das Sarma[1]

AUTHOR AFFILIATION See affiliation list on p. 17.

ABSTRACT β-coronaviruses cause acute infection in the upper respiratory tract, resulting in various symptoms and clinical manifestations. OC43 is a human β-coronavirus that induces mild clinical symptoms and can be safely studied in the BSL2 laboratory. Due to its low risk, OC43 can be a valuable and accessible model for understanding β-coronavirus pathogenesis. One potential target for limiting virus infectivity could be gap junction-mediated communication. This study aims to unveil the status of cell-to-cell communications through gap junctions in human β-coronavirus infection. Infection with OC43 leads to reduced expression of Cx43 in A549, a lung epithelial carcinoma cell line. Infection with this virus also shows a significant ER and oxidative stress increase. Internal localization of Cx43 is observed post-OC43 infection in the endoplasmic reticulum–Golgi intermediate compartment (ERGIC) region, which impairs the gap junction communication between two adjacent cells, confirmed by Lucifer yellow dye transfer assay. It also affects hemichannel formation, as depicted by the EtBr uptake assay. Impairment of Cx43 trafficking and the ability to form hemichannels and functional GJIC are hampered by virus-induced Golgi apparatus disruption. Altogether, these results suggest that several physiological changes accompany OC43 infection in A549 cells and can be considered an appropriate model system for understanding the differences in gap junction communication post-viral infections. This model system can provide valuable insights for developing therapies against human β-coronavirus infections.

IMPORTANCE The enduring impact of the recent SARS-CoV-2 pandemic underscores the importance of studying human β-coronaviruses, advancing our preparedness for future coronavirus infections. As SARS-CoV-2 is highly infectious, another human β-coronavirus OC43 can be considered an experimental model. One of the crucial pathways that can be considered is gap junction communication, as it is vital for cellular homeostasis. Our study seeks to understand the changes in Cx43-mediated cell-to-cell communication during human β-coronavirus OC43 infection. *In vitro* studies showed downregulation of the gap junction protein Cx43 and upregulation of the endoplasmic reticulum and oxidative stress markers post-OC43 infection. Furthermore, HCoV–OC43 infection causes reduced Cx43 trafficking, causing impairment of functional hemichannel and GJIC formation by virus-mediated Golgi apparatus disruption. Overall, this study infers that OC43 infection reshapes intercellular communication, suggesting that this pathway may be a promising target for designing highly effective therapeutics against human coronaviruses by regulating Cx43 expression.

KEYWORDS OC43, human β-coronavirus, gap junction communication, connexin 43, Golgi apparatus disruption

Gap junction intercellular communication (GJIC) maintains cellular homeostasis in multicellular organisms by allowing cells to coordinate and respond to signals. Gap junctions are specialized channels that exchange ions, signaling molecules, and

small molecules (especially less than 1 kDa) between adjacent cells (1). This connection aids in rapid and synchronized cellular responses critical for various physiological processes. Gap junctions are formed with protein subunits called connexons, comprising a hexameric assembly of connexins. When present on the cell surface, these connexons develop hemichannels that make these cells susceptible to external stimuli. The coupling of the connexon from one cell with the connexon of another cell generates functional gap junctions (2). These gap junctions in their open conformations provide a passage between adjacently present cells, which facilitates the passive diffusion of essential molecules to maintain cellular homeostasis (3).

The expression of gap junction proteins, particularly connexin, is modulated following virus infections (4–6). Connexin 43 (Cx43), the most ubiquitously expressed and widely studied among all connexins, has been extensively studied in response to murine β-coronavirus infections (7–10). The regulation in Cx43 following virus infection is attributed to either viral burden on the endoplasmic reticulum (ER), causing cellular stress, or hijacking microtubule-mediated transport for trafficking of viral proteins within the cells. Virus burdens the endoplasmic reticulum of the host cell by translating a large number of viral proteins (11). Virus-induced ER stress can alter host cellular processes, potentially causing cellular damage. ER stress can be detected by different host cell markers, including heat shock factor (HSF1), heat shock protein 70 (HSP70), and endoplasmic reticulum protein 29 (ERp29). Under ER stress, HSF1 regulates the production of HSP70, a chaperone, by binding to the heat shock elements (HSE) (12). HSP70 stabilizes unfolded proteins through selective binding, thus preventing aggregate formation, while parallelly facilitating refolding of misfolded proteins (13, 14). ERp29 is a major chaperone protein that helps in the trafficking of membrane proteins to the cell surface, including Cx43 (15). In addition to its role in protein trafficking, overexpression of ERp29 induced by ER stress significantly contributes toward overall unfolded protein stress. More specifically, ERp29-mediated activation of protein-degrading machinery aids in the clearance of denatured proteins and prevents protein aggregation (16). Recent evidence has demonstrated that viral infections are coupled with an increase in the production of reactive oxygen species (ROS), which the host cannot combat. Resultant oxidative stress generated in the host cell can be detected by regulation of Parkinson disease protein 7, DJ-1. DJ-1 has roles in transcriptional regulation and antioxidative stress reaction, which helps recover from oxidative stress (17, 18).

This study employs the HCoV–OC43 virus to elucidate the effect of viral infection in modulating gap junction-mediated cell-to-cell communication in a human lung epithelial cell line, A549. OC43 is a human β-coronavirus that causes mild symptoms in humans and hence can be a suitable model for understanding the pathogenesis caused by the infections of human coronaviruses. OC43 shares many similarities with respect to genome size, transmission mode, common symptoms, and pathogenesis with other human β-coronaviruses, including SARS-CoV-2. Studies on human coronaviruses are needed because of the lack of available human data and the reproducibility of pathogenesis in other virus models. Hence, studying β-coronaviruses in human models is essential, and OC43 can be an excellent option. Here, we used a human lung epithelial cell line, A549, to understand the changes in functional gap junction and hemichannel formation post-OC43 infection. We observed that post-infection, Cx43 is reduced at the protein level, accompanied by an increase in ER and oxidative stress markers. Cx43 is retained in the perinuclear region of infected cells, confirmed by immunofluorescence and Triton X-100 solubilization assay. With the decrease in Cx43, the cells could not form functional gap junctions and hemichannels, confirmed by the Lucifer yellow dye transfer assay and the ethidium bromide uptake assay. The formation of functional hemichannel and gap junctions is hindered by HCoV–OC43-mediated Golgi apparatus disruption. These data suggest that targeting Cx43 to modulate its expression can be a valuable therapeutic target to reduce β-coronavirus infections.

MATERIALS AND METHODS

Reagents and antibodies

Bicinchoninic acid (BCA) protein assay kits and SuperSignal West Pico PLUS Chemilumi-nescent Substrate were procured from Thermo Fisher Scientific. Protease and phosphatase inhibitor cocktails were obtained from Sigma-Aldrich. Cell culture reagents, including Dulbecco's modified Eagle medium (DMEM), fetal bovine serum (FBS), 0.25% trypsin, and penicillin/streptomycin, were obtained from Gibco. Primary antibodies used in the study are listed in Table 1, and the secondary antibodies used are listed in Table 2. The remaining chemicals were procured from Merck (Deu, Germany), SRL (MB, India), Sigma-Aldrich (MO, USA), or Thermo Fisher Scientific (MA, USA). The mouse monoclonal antibody (MAbs 1–10C.3), which is directed against the surface spike glycoprotein of HCoV–OC43 (19–23), was a kind gift from Dr. Brenda Hogue (Arizona State University, AZ, USA).

Cells and viruses

The human epithelial lung carcinoma cell line A549 was obtained from Dr. Michael Koval (Emory University School of Medicine, Atlanta, Georgia, USA), and African green monkey kidney epithelial cells, Vero cells, were a kind gift from Dr. Sourish Ghosh (Indian Institute of Chemical Biology, Kolkata, West Bengal, India). The human cervical cancer cell line HeLa was purchased from ATCC (American Type Culture Collection). The cell lines were maintained in DMEM supplemented with 10% heat-inactivated FBS and 1% penicillin and streptomycin. The cells were maintained at 37°C in a humidified incubator with 5% CO_2. Human coronavirus OC43 (HCoV–OC43) was obtained through BEI Resources, NIAID, NIH (catalog number: NR-56241). The virus was propagated in Vero cells for further use.

Virus propagation and virus infection

For virus propagation, a 60-mm dish of around 80% confluent Vero cells was inoculated with OC43 at a multiplicity of infection (MOI) of 1 in 500 µL of infection media (DMEM supplemented with 2% FBS and 1% penicillin and streptomycin). The virus was allowed to adsorb onto the cells for 2 hours with intermediate shaking after 15-minute intervals at 33°C in a humidified incubator with 5% CO_2. The infection medium was removed after 2 hours, and 2.5 mL of infection media was added. The plate was incubated for 4 days at 33°C with 5% CO_2. Four days were chosen for virus incubation based on the cytopathic effects exhibited by the virus on Vero cells. The medium was collected from the dish and

TABLE 1 Primary antibodies used in this study

No.	Primary antibody	Application	Dilution	Source
1	Anti-Cx43 (polyclonal)	WB	1:2000	Abclonal, MA, USA
2	Anti-HSP70 (polyclonal)	WB	1:1000	Bio-Bharati Life Science Pvt. Ltd, India
3	Anti-HSF1 (polyclonal)	WB	1:1000	Bio-Bharati Life Science Pvt. Ltd, India
4	Anti-GAPDH (polyclonal)	WB	1:5000	Bio-Bharati Life Science Pvt. Ltd, India
5	Anti-ERp29 (polyclonal)	WB	1:1000	Invitrogen, MA, USA
6	Anti-DJ1	WB	1:500	Bio-Bharati Life Science Pvt. Ltd, India
7	Anti-β-actin (polyclonal)	WB	1:5000	Bio-Bharati Life Science Pvt. Ltd, India
8	Anti-γ-actin (polyclonal)	WB	1:5000	Bio-Bharati Life Science Pvt. Ltd, India
9	Anti-Cx43 (polyclonal)	IF	1:1000	Sigma-Aldrich, MO, USA
10	Anti-Cx43 (monoclonal)	IF	1:100	Sigma-Aldrich, MO, USA
11	Anti-OC43 (monoclonal)	IF	1:50	Kind gift from Dr. Brenda Hogue (Arizona State University, AZ, USA)
12	Anti-calnexin	IF	1:100	Enzo Life Sciences, Inc., NY, USA
13	Anti-COPB2	IF	1:100	Abclonal, MA, USA
14	Anti-TGN46	IF	1:100	Abclonal, MA, USA

TABLE 2 Secondary antibodies used in this study

No.	Secondary antibody	Application	Dilution	Source
1	Alexa Fluor 488 Goat Anti-Rabbit	IF	1:1000	Invitrogen, MA, USA
2	Alexa Fluor 488 Goat Anti-Mouse	IF	1:1000	Invitrogen, MA, USA
3	Alexa Fluor 568 Donkey Anti-Rabbit	IF	1:1000	Invitrogen, MA, USA
4	Alexa Fluor 568 Donkey Anti-Mouse	IF	1:1000	Invitrogen, MA, USA
5	HRP conjugated Rabbit secondary antibody	WB	1:10000	Invitrogen, MA, USA

centrifuged at 500 g for 5 minutes to clarify the viral particles. The supernatant obtained was aliquoted and kept at −80°C for further use. For virus infection, 80% confluent A549 cells were inoculated with OC43 at MOI 0.5 and 1 in infection media. The virus inoculum was adsorbed for 2 hours at 37°C, 5% CO_2, with shaking every 15 minutes. The inoculum was removed after 2 hours, and fresh infection medium was added. The cells were incubated at 37°C with 5% CO_2.

Viral titer determination by the TCID50 assay

Vero cells were plated in a 96-well plate and incubated at 37°C with 5% CO_2 till the cells were 70%–80% confluent. The medium was removed from the wells and washed with PBS. The PBS was removed, and the cells were inoculated with ten-fold serial dilutions of OC43 stock virus. Hundred microliters of the dilutions was added to each well, and the plate was incubated for 6 days at 37°C with 5% CO_2. After 6 days, the plate was removed, and the medium was discarded. At room temperature, the cells were fixed in 4% paraformaldehyde (4% PFA) for 15 minutes. The cells were permeabilized with 0.2% Triton X-100 in PBS after fixation. A blocking solution of 50 µL was added using 2.5% heat-inactivated goat serum in PBS with 0.2% Triton X-100. The incubation was carried out for 15 minutes at room temperature. Twenty-five microliters of the primary antibody diluted in the blocking solution was added to the wells and was incubated for 2 hours at room temperature. Similarly, after washing, 25 µL of the secondary antibody (Alexa Fluor 488 Goat Anti-Mouse) 1:1000 diluted in the blocking solution was added to the wells and incubated for 1 hour 15 minutes at room temperature. The wells were washed, and images were taken using a 10X objective in a Nikon Eclipse Ts2-FL microscope (Tokyo, Japan) and device camera Nikon DS-Fi3 (Tokyo, Japan). The Reed–Muench method was used for calculation of TCID50 (24). To convert the TCID50/mL values to PFU/mL, TCID50/mL values were multiplied by 0.7 (25).

Immunofluorescence

A549 cells were grown on etched coverslips, and virus infection was performed. After infection, cells were washed with wash buffer (PBS with calcium and magnesium). PFA (4%) was used for cell fixation for 10 minutes at room temperature. To permeabilize the cells, PBS, along with 0.2% Triton X-100, was used. Following permeabilization, cells were blocked using a blocking solution made of 2.5% heat-inactivated goat serum in PBS with 0.2% Triton X-100. The primary antibody was diluted in the blocking solution, and 30-µL drops were applied on a surface where the coverslips were inverted. The setup was placed in a humidified chamber overnight at 4°C. After washing, the coverslips were similarly placed on drops of the secondary antibody and incubated for 1 hour 15 minutes at room temperature. Cells were washed and mounted in Mowiol containing DAPI to stain the nucleus. The slides were imaged in an Olympus IX-81 microscope, a Zeiss Confocal Laser Scanning Microscope (LSM710), or a Leica SP8 confocal microscope. Images were processed with ImageJ (NIH), Zen 3.7 (Carl Zeiss AG), or LAS X (Leica Microsystems) software.

Protein isolation and immunoblotting

Cultured cells were subjected to virus infections and incubated for 3 days for protein extraction. After 3 days, the medium was discarded and rinsed twice with ice-cold PBS.

RIPA buffer was used for cell lysis which comprised 50 mM Tris, 150 mM NaCl, 0.1% sodium dodecyl sulfate (SDS), 0.5% sodium deoxycholate ($C_{24}H_{40}O_4$), 1% Triton X-100, EDTA-free complete protease, and phosphatase inhibitors (1 mM sodium orthovanadate, 10 mM sodium fluoride, and 10 mM sodium pyrophosphate decahydrate). The cell lysis process was conducted on ice for 1 hour and 30 minutes, with intermittent vortexing every 15 minutes. Centrifugation at 13,200 rpm for 20 minutes at 4°C was performed using an Eppendorf 5415 R centrifuge to clarify the cell lysate. The pellet was discarded, and the supernatant was collected as it contained the cellular proteins, and the total protein concentration was estimated. It was determined using a Pierce® BCA Protein Assay Kit (Thermo Scientific, Rockford, IL, USA) following the manufacturer's instructions. An equal amount of protein was subsequently separated by 12% SDS-PAGE and then transferred onto a polyvinylidene difluoride (PVDF) membrane (Millipore, Bedford, MA). The membrane was blocked with a 5% skimmed milk solution prepared in Tris-buffered saline containing 0.1% Tween-20 (TBS-T) for 1 hour at room temperature. The membrane was then incubated overnight at 4°C with primary antibody solutions diluted in the blocking solution. After the primary antibody incubation, the membrane was washed thrice with TBS-T for 10 minutes each. Subsequently, it was incubated at RT for 1 hour with an appropriate secondary antibody conjugated with horseradish peroxidase (HRP) prepared in a blocking solution. After washing with TBS-T, immunoreactive bands were visualized using the SuperSignal West Pico PLUS Chemiluminescent Substrate (Thermo Scientific) following the manufacturer's instructions. Images of the blots were captured with the help of GENESys software (Genesys, Cambridge, UK) with the Syngene G: Box ChemiDoc system. The membranes were re-probed with anti-GAPDH, anti-β-actin, or anti-γ-actin antibodies to ensure equal protein loading. Densitometric analysis of the obtained bands was performed using ImageJ software.

Triton X-100 solubilization assay

Cells were collected by scraping in PBS containing protease and phosphatase inhibitors. The cell suspension obtained was passed through a Dounce homogenizer 100 times. The cell homogenate was centrifuged for 5 minutes at 500 g using an Eppendorf 5415 R centrifuge, maintaining a temperature of 4°C. The supernatant was collected in ultracentrifuge tubes and centrifuged at 100,000 g for 30 minutes, maintaining the temperature at 4°C using a ThermoFisher Sorvall WX 100+ ultracentrifuge with a ThermoFisher TFT-80.2 fixed angle rotor. The membrane-enriched pellet obtained was resuspended in ice-cold PBS containing 1% Triton X-100 and was incubated for 30 minutes, strictly maintaining a temperature of 4°C. After incubation, the samples were centrifuged at 100,000 g for 30 minutes at 4°C. The supernatant obtained corresponds to the Triton X-100 soluble fraction, and the pellet obtained was considered insoluble. The equal volumes of soluble and insoluble fractions, diluted in Laemmli sample buffer, were resolved by SDS-PAGE followed by Cx43 immunoblotting.

Lucifer yellow dye transfer assay

Cultured, mock, and infected cells grown in 12-well plates were washed with PBS. A uniform release of 10 µL of Lucifer yellow dye (4 mg/mL concentration) was performed, while generating a scratch in the cell monolayer to perform the scrape loading assay (7). The plate was incubated at room temperature for 1 minute, followed by washing in PBS. Subsequently, PBS was added to the wells, and the plate was incubated at 37°C for 10 minutes to facilitate the diffusion of the loaded dye to the neighboring cells. After incubation, cells were fixed using 4% PFA for 10 minutes at room temperature. Images were captured using an Olympus IX-81 microscope operating at 10X magnification with 488 nm excitation. The distance traveled by the dye was measured with the help of ImageJ (NIH, USA) software (26).

Ethidium bromide (EtBr) dye uptake assay

Cells cultured on etched coverslips in a 24-well plate were washed twice with Locke's solution, comprising 154 mM NaCl, 5.4 mM KCl, 2.3 mM CaCl2, and 5 mM HEPES buffer at a pH of 7.4. After washing twice, a 5-µm ethidium bromide (EtBr) solution prepared in Locke's solution was added to the wells (27). The plate was incubated for 10 minutes at 37°C. The cells were fixed with 4% PFA for 10 minutes at room temperature. Subsequently, the cells were washed with Locke's solution, and the coverslips containing cells were mounted in a Mowiol mounting medium that did not contain DAPI. Images were captured using an Olympus IX-81 microscope operating at 40X magnification. The intensity of EtBr uptake by cells was measured with the help of ImageJ (NIH, USA) software (26).

Data and statistical analyses

The data from all experiments are presented in the form of mean values accompanied by their standard error of the mean (mean ± SEM). Statistical analysis was performed using a two-tailed student's t-test with Welch's correction. Statistical significance was attributed to results with a P value of < 0.05. GraphPad Prism 8 software (GraphPad Software, Inc.) was employed for all statistical analyses.

RESULTS

Viral growth kinetics in A549 cells and validation of the anti-OC43 antibody

For investigating the viral infection and transmission in A549 cells, the cells were infected with OC43 at MOIs 0.5 and 1, and immunofluorescence staining with the anti-OC43 antibody was performed at days 2, 3, and 4 post-infection (p.i.) (Fig. 1A through F). Day 3 p.i. showed maximum virus infection spread, and on day 4 p.i., some of the cells started to die; hence, the infection spread is comparatively lower than on day 3 p.i., as quantified using ImageJ software (Fig. 1G). A similar extent of infection was observed in the case of MOIs 0.5 and 1 on day 3 post-infection and were chosen for further experiments.

To validate the anti-OC43 antibody, transient transfection of the OC43 spike protein in HeLa cells was performed followed by immunofluorescence staining. HeLa cells were plated on etched coverslips in a 24-well plate and were grown till they reached a confluency of 80%–90%. The cells were transfected with the plasmid-expressing HCoV–OC43 spike protein (OC43-S-Y/pCAGGS) using Lipofectamine 2000 (Invitrogen, Carlsbad, CA) at a Lipofectamine/DNA ratio of 3:1 (28). An immunofluorescence staining experiment was performed where controls (Fig. 1H through J) and transfected (Fig. 1K through M) cells were incubated with the anti-OC43 antibody for 1.5 hours at room temperature and labeled with Alexa Fluor 568 Donkey Anti-Mouse. The images were captured in an Olympus IX-81 microscope. The images revealed that the signal from the anti-OC43 antibody could be perceived from the cells expressing the YFP-tagged OC43 spike protein (Fig. 1K through M). This suggests that the antibody used in this study is specific toward the spike protein of OC43.

Reduced Cx43 protein expression post-OC43 virus infection

Immunofluorescence imaging and immunoblotting were performed to determine the effect of OC43 infection on the expression of gap junction protein Cx43 in A549 cells. For immunofluorescence, A549 cells grown on etched coverslips were infected with OC43 at different MOIs of 0.1 and 0.5. Immunostaining was performed at day 3 p.i. using rabbit anti-Cx43 and mouse anti-OC43 antibodies. The images were captured in a Zeiss Confocal Laser Scanning Microscope (LSM710) (Fig. 2A through L). It is observed that non-infected cells express punctate staining of Cx43 throughout, depicted with white arrows (Fig. 2C, G and K). The infected cells, depicted with yellow arrows, show reduced punctate staining, suggesting an overall downregulation in Cx43 expression (Fig. 2G and K). The green arrows depict the perinuclear localization of Cx43 in infected cells (Fig. 2G
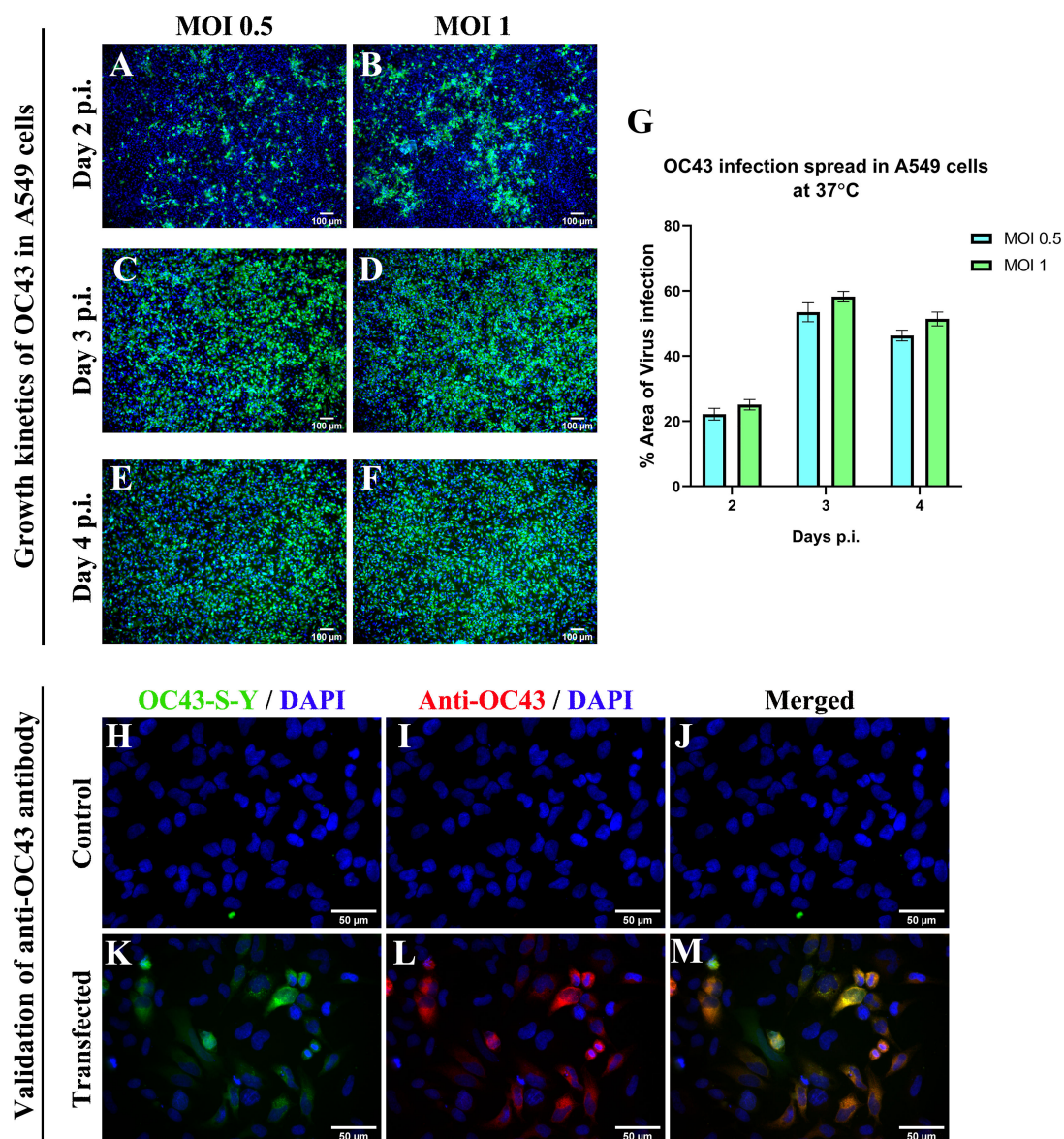
FIG 1 Viral infection in A549 cells on different days p.i. Infection with OC43 in A549 cells was standardized based on the immunofluorescence staining of virus spread. A549 cells were infected with MOIs 0.5 and 1 of OC43, fixed at different time points, immunostained, and imaged in an IX-81 microscope (A-F) The infection spread was quantified using ImageJ software and plotted using the absolute percentage area of virus infection (G). Data expressed as mean ± SEM of three individual experiments. To confirm the specificity of the anti-OC43 antibody, HeLa cells were transiently transfected with a plasmid expressing the HCoV–OC43 spike protein. The cells were transfected using Lipofectamine 2000 at a ratio of 3:1 (Lipofectamine/DNA). Microscopic imaging of control (H-J) and transfected (K-M) cells using an Olympus IX-81 microscope showed a detectable signal from the anti-OC43 antibody in cells expressing the YFP-tagged OC43 spike protein, thus confirming the specificity of the antibody toward the OC43 spike protein. The scale bar of the images (A-F) depicts 100 microns, and images (H-M) depict 50 microns.

and K). To confirm the Cx43 expression level alteration, immunoblotting was performed with the rabbit anti-Cx43 antibody, and the membrane was stripped and re-probed with the rabbit anti-GAPDH antibody to ensure equal loading (Fig. 2M). With the help of densitometric analysis used in ImageJ software, it is observed that OC43 infection affects the expression of Cx43 (Fig. 2N). This suggests that upon OC43 infection in A549 cells, the gap junction communication protein Cx43 is downregulated.

Determination of co-localization between the OC43 spike protein and Cx43 was done through immunofluorescence (Fig. 3). Different microscopic fields and their Z-stacks were considered for this analysis. Representative Z-stacks and their colocalizing points of
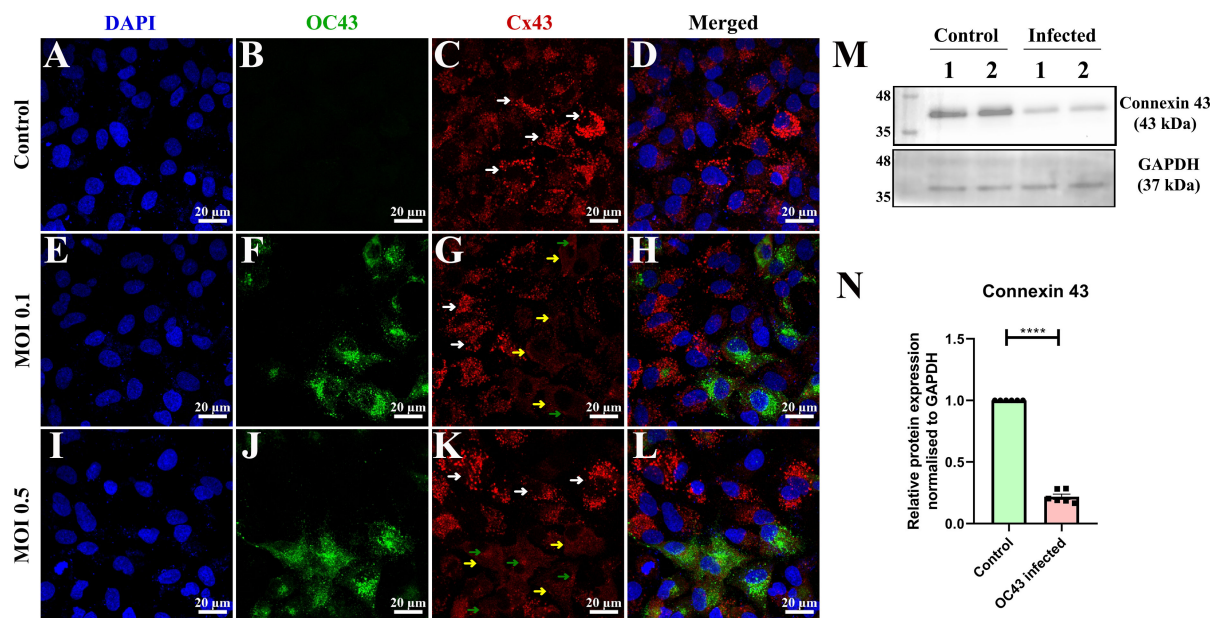
FIG 2 Connexin 43 expression in control and HCoV-OC43 infected A549 cells. A549 cells were immunostained with the anti-OC43 antibody and anti-Cx43 antibody and counterstained with DAPI. Images correspond to different sets, such as control (A-D), OC43-infected MOI 0.1 (E-H), and OC43-infected MOI 0.5 (I-L). The non-infected cells showing punctate staining of Cx43 are marked with white arrows (C, G, and K), and the OC43-infected cells showing reduced Cx43 punctate staining are marked with yellow arrows (G and K). Infected cells showing perinuclear Cx43 staining are marked with green arrows (G and K). D, H, and L represent merged images of the different channels. A Western blot, using 10 µg of protein loaded per well, determined the overall expression of connexin 43 (M).Results of densitometric analysis using ImageJ software of the bands obtained were plotted (N). Control and infected lanes marked as 1 and 2, respectively, represent technical replicates. Data expressed as mean ± SEM of three individual replicates. The significant differences are indicated by *$P < 0.05$, **$P < 0.01$, ***$P < 0.001$, and ****$P < 0.0001$. The scale bar for all the images is 20 microns.

different sets are shown in Fig. 3A through X. Co-localization analysis comparing Pearson's correlation coefficient (Fig. 3Y) revealed that in both MOI 0.1 and MOI 0.5, a low but positive correlation can be found, depicting possible co-localization of the OC43 spike protein and Cx43.

HCoV-OC43 infection in A549 cells increases ER and oxidative stress

A549 cells were infected with MOI 1 and incubated for 3 days p.i. Total protein was isolated and estimated using the BCA assay. Ten micrograms of the protein was loaded in each well for control and OC43-infected samples. We checked the ER stress and oxidative stress in control and infected samples. HSF1, HSP70, and ERp29 were chosen as ER stress markers, and DJ-1 was selected as the oxidative stress marker. As observed by the upregulation of ER stress markers, infection with HCoV–OC43 in A549 cells increased ER stress (Fig. 4A through D). The oxidative stress marker, DJ-1, shows a trend in upregulation, though statistically nonsignificant (Fig. 4A and E). These results suggest that upon OC43 infection, there is an overall increase in cellular stress.

Internal localization of Cx43 upon HCoV–OC43 infection

We determined the localization of Cx43 in mock-infected and infected A549 cells. Immunofluorescence staining in Fig. 2 shows the infected cells with reduced punctate staining and perinuclear localization of Cx43, depicted by green arrows (Fig. 2G and K). The reduction of Cx43 in gap junctional plaques upon virus infection was confirmed by the Triton X-100 solubilization assay. The densitometric analysis of infected samples showed a significant decrease in the ratio of Triton X-100 insoluble to soluble levels of Cx43 when compared to control samples (Fig. 5A and B). This further indicates increased Cx43 gap junction assembly at the cell surface in mock-infected samples compared to infected samples.
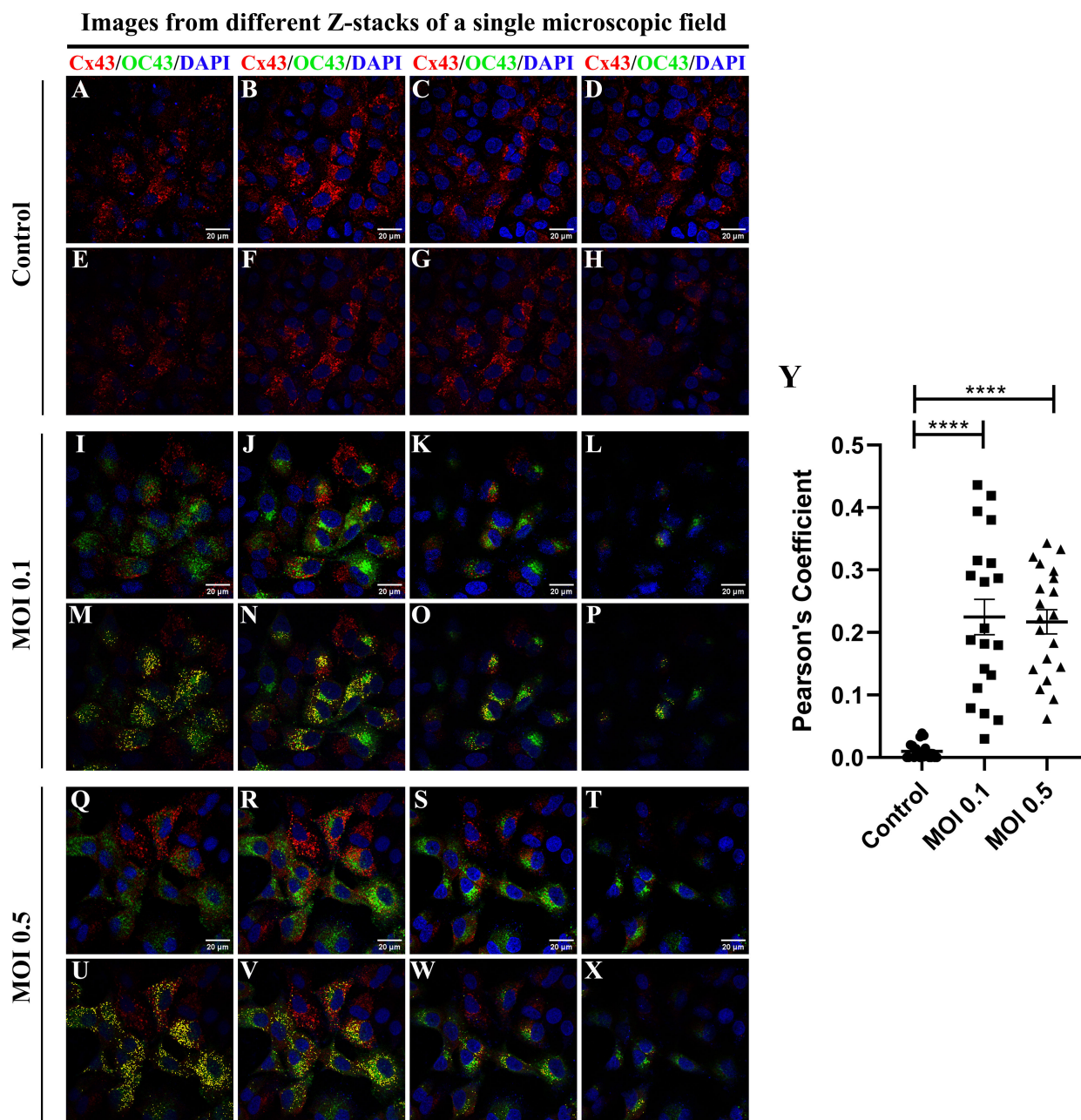
FIG 3 Colocalization of the OC43 spike protein with Cx43 in A549-infected cells. A549 cells were immunostained with anti-OC43 and anti-Cx43 antibodies and were counterstained with DAPI. Images shown correspond to different sets, such as control (A-H), A549 cells infected at MOI 0.1 (I-P), and at MOI 0.5 (Q-X). Images shown in each of the panels for control (A-D), MOI 0.1 (I-L), and MOI 0.5 (Q-T) represent different Z-stack positions of a microscopic field. The images E–H, M–P, and U–X show the colocalizing points within the Z-stacks, which are highlighted in yellow. Graph Y represents Pearson's correlation coefficient of different sets. The significant differences are indicated by *$P < 0.05$, **$P < 0.01$, ***$P < 0.001$, and ****$P < 0.0001$. The scale bar for all the images is 20 microns.

To identify the subcellular localization of Cx43 upon OC43 infection, we performed immunostaining of an ER resident protein, calnexin, using rabbit anti-calnexin antibody and ERGIC marker, COPB2, using the rabbit anti-COPB2 antibody. Confocal images showed that infected cells have perinuclear connexin staining (Fig. 6F and N). The non-infected cells are marked with white arrows, and the infected cells are marked with yellow arrows (Fig. 6F, H, N and P). Visual analysis of the microscopic images reveals that the perinuclear localization of Cx43 in infected cells coincides with the positioning of ERGIC marker COPB2 (Fig. 6P).
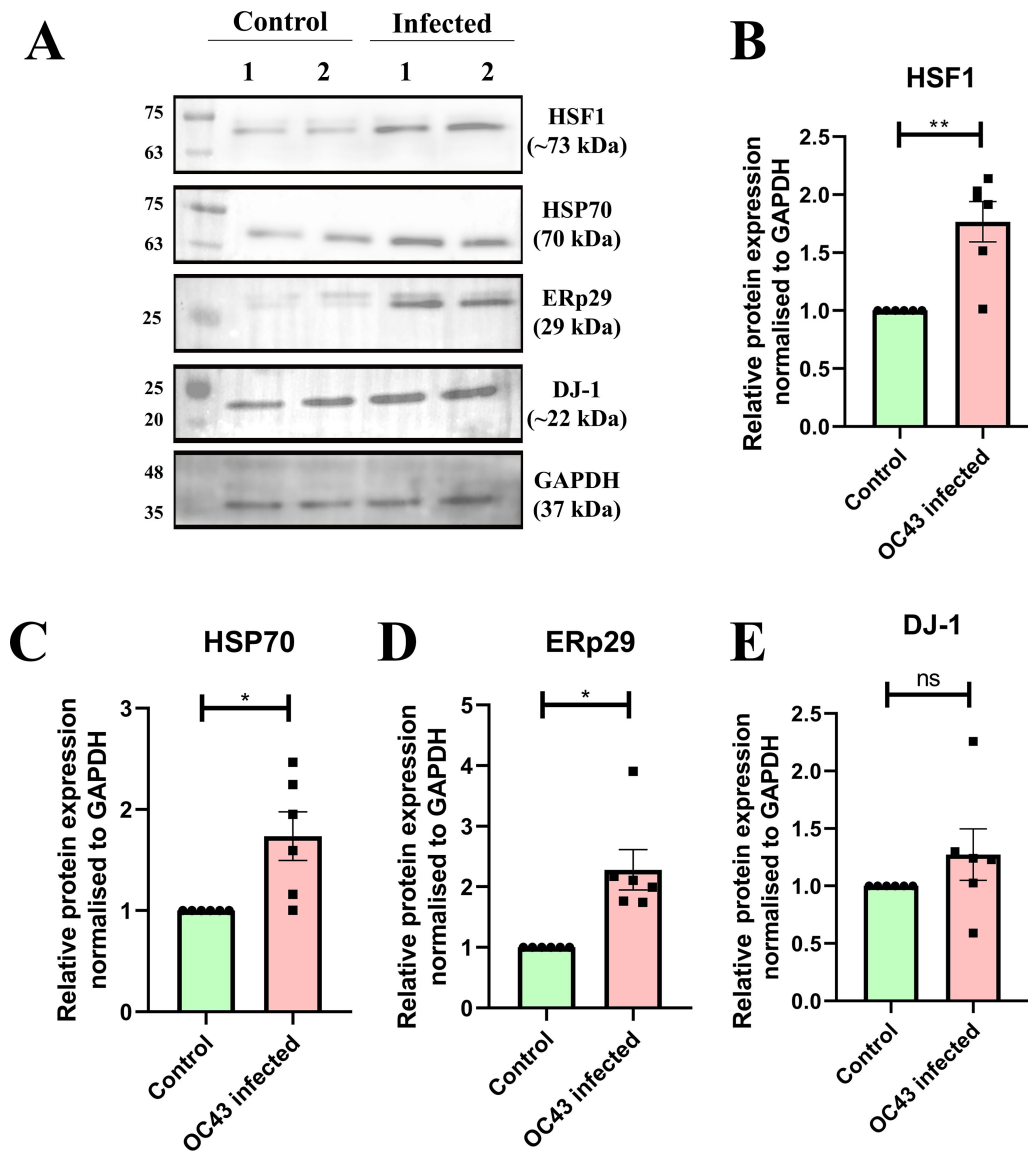
FIG 4 HCoV–OC43 induces ER stress and oxidative stress in A549 cells. Western blot analysis was performed using 10 µg of protein loaded per well to determine the expression of different stress markers. Representative immunoblots show the upregulation of different stress markers in infected samples compared to control (A). Scatterplots representing the densitometric analysis of the different stress markers normalized to the loading control GAPDH (B-E). (B) represents significant upregulation of HSF1, (C) represents upregulation of HSP70, (D) represents significant upregulation of ERp29, and (E) represents a trend in upregulation of DJ-1. Control and infected lanes marked as 1 and 2, respectively, represent technical replicates. Data expressed as mean ± SEM of three individual replicates. The significant differences are indicated by *$P < 0.05$, **$P < 0.01$, ***$P < 0.001$, and ****$P < 0.0001$.

Functional gap junction and hemichannels are impaired in A549 cells post-HCoV–OC43 infection

Cx43 can function as a gap junction channel and also as a hemichannel. As previously determined upon HCoV–OC43 infection in A549 cells, Cx43 is localized in the ERGIC compartment. Due to the depletion of surface Cx43, gap junction and hemichannel communication gets impaired. Functional gap junction intercellular communication (GJIC) is determined with the help of Lucifer yellow (LY) dye transfer assay. GJIC allows the passage of molecules less than 1 kDa in weight (29). LY is a small dye with a molecular weight of around 450 Daltons (30). The LY dye can be transferred from one adjacent
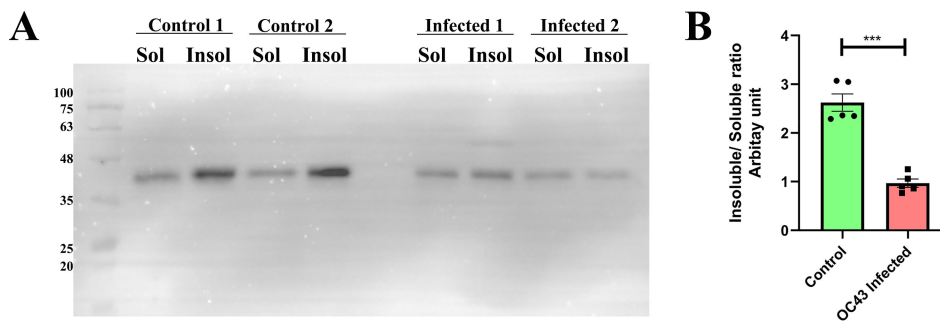
FIG 5 HCoV–OC43 infection in A549 cells impairs Cx43 trafficking to the cell surface. To confirm the internal localization of Cx43 upon OC43 infection, a Triton X-100 solubilization assay was performed (A), and the densitometric analysis of the bands obtained revealed that the Insol/sol fraction of the control is greater than that of the infected samples (B). Data expressed as mean ± SEM of three individual replicates. The significant differences are indicated by *$P < 0.05$, **$P < 0.01$, ***$P < 0.001$, and ****$P < 0.0001$.

cell to another with the help of functional GJIC. We investigated the status of GJIC in control and OC43-infected A549 cells using the LY dye transfer assay. An observation in control cells showed that the LY dye was absorbed more than OC43-infected cells (Fig. 7A through F). The distance traveled by the LY dye from scratch was measured, and the absolute values in microns were plotted (Fig. 7G). From the graph observed, it is inferred that the GJIC is impaired in the case of HCoV–OC43 infection. Ethidium bromide (EtBr) dye uptake assay was performed to identify the presence of functional hemichannels in control and infected A549 cells. The cells were incubated with EtBr in Locke's solution. The control cells exhibit a brighter EtBr signal (Fig. 7H) than OC43-infected cells (Fig. 7I), depicting a higher level of hemichannel activity (Fig. 7J). In conclusion, the restricted access of Cx43 on the cell surface in HCoV–OC43-infected A549 cells disrupts GJIC and hemichannel activity.

Disruption of Golgi apparatus post-HCoV–OC43 infection in A549 cells

To understand the mechanism of Cx43-mediated GJIC impairment, immunofluorescence staining and Western blot studies were performed to check the status of the Golgi apparatus. For the immunofluorescence study, A549 cells were grown on etched coverslips and were infected with OC43 MOI 1. Immunostaining was performed with anti-TGN46 and anti-OC43 antibodies. The representative immunostained images are shown in Fig. 8A through F. The white arrows in Fig. 8E depict OC43-infected A549 cells with either complete loss of TGN46 staining or disrupted TGN46 staining. To check the percentage of infected cells showing TGN46 staining, a total of 500 cells from both control and infected were considered from different microscopic fields, and cells expressing TGN46 staining were counted. A graph depicting approximately 97.1% of non-infected cells and 13.1% of infected A549 cells shows the presence of TGN46 staining (Fig. 8G). The disruption of the Golgi apparatus was further studied by Western blot analysis (Fig. 8H). Densitometric analysis of the bands obtained through ImageJ software revealed that the infected cells show reduced TGN46 protein expression. The data are depicted as a scatterplot in Fig. 8I. Overall, these experiments confirm the disruption of the Golgi apparatus post-HCoV–OC43 infection in A549 cells.

Disruption of Golgi apparatus is responsible for reducing Cx43 punctate staining and increased localization with COPB2

To determine the effect of virus-induced Golgi apparatus disruption on Cx43 protein expression and localization, immunofluorescence staining and Western blot analysis were performed with Brefeldin A (BFA)-treated A549 cells. A549 cells were treated with 0.2 µg/mL BFA and were incubated for 24 hours. An immunofluorescence staining study with anti-Cx43 and anti-TGN46 antibodies revealed that upon Golgi apparatus
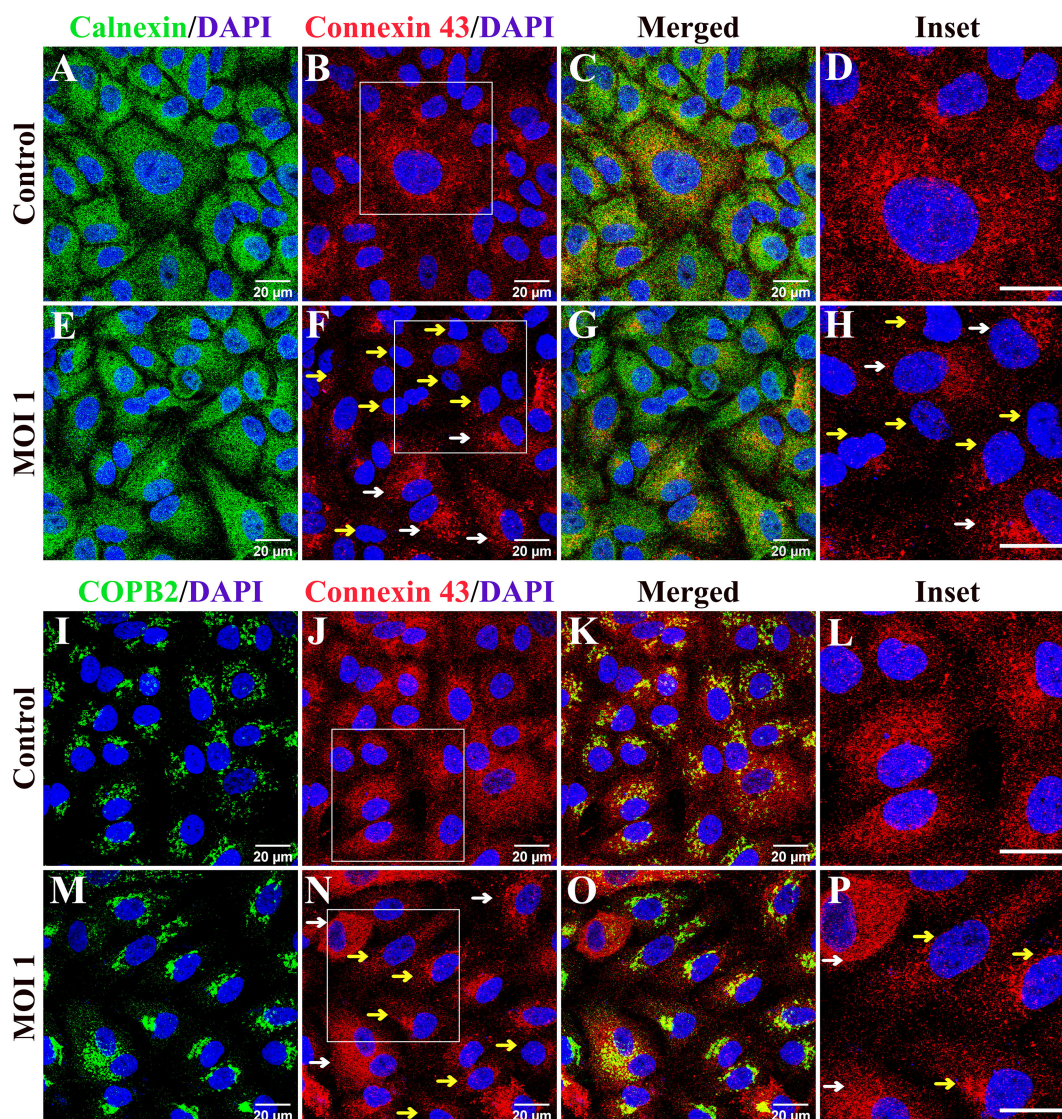
FIG 6 Cx43 localizes in the ERGIC region post-OC43 infection in A549 cells. To determine the internal localization of Cx43 post-infection in subcellular compartments, control and infected cells were immunostained with anti-calnexin (A-H) and anti-COPB2 (I-P) The control cells expressing Cx43 staining are marked with white arrows, and the infected cells with perinuclear Cx43 are marked with yellow arrows (F, H, N, and P). Upon visual observation, it is inferred that, upon OC43 infection, Cx43 trafficking is impaired and localizes in the ERGIC compartment of the cells. The insets are digitally zoomed. The scale bar for all the images is 20 microns.

disruption, the punctate staining of Cx43 is greatly reduced (Fig. 9A through F). The white arrows depict the punctate staining of Cx43 in control cells (Fig. 9A), whereas the yellow arrows depict the BFA-treated cells where reduced Cx43 punctate staining was observed (Fig. 9D). A Western blot analysis and the densitometric analysis of the bands obtained showed that Cx43 protein expression is significantly downregulated in case of Golgi apparatus disruption (Fig. 9G and H). Further, the localization of Cx43 was tested in control and BFA-treated cells. Colocalization studies revealed that upon BFA treatment, the Cx43 localization in the ERGIC compartment is significantly increased, as can be seen from the images in Fig. 9I through P and in the scatterplot in Fig. 9Q. Overall, these experiments confirm that virus-induced Golgi apparatus disruption can be one of the mechanisms through which Cx43 expression, localization, and function are being modulated post-HCoV–OC43 infection in A549 cells.
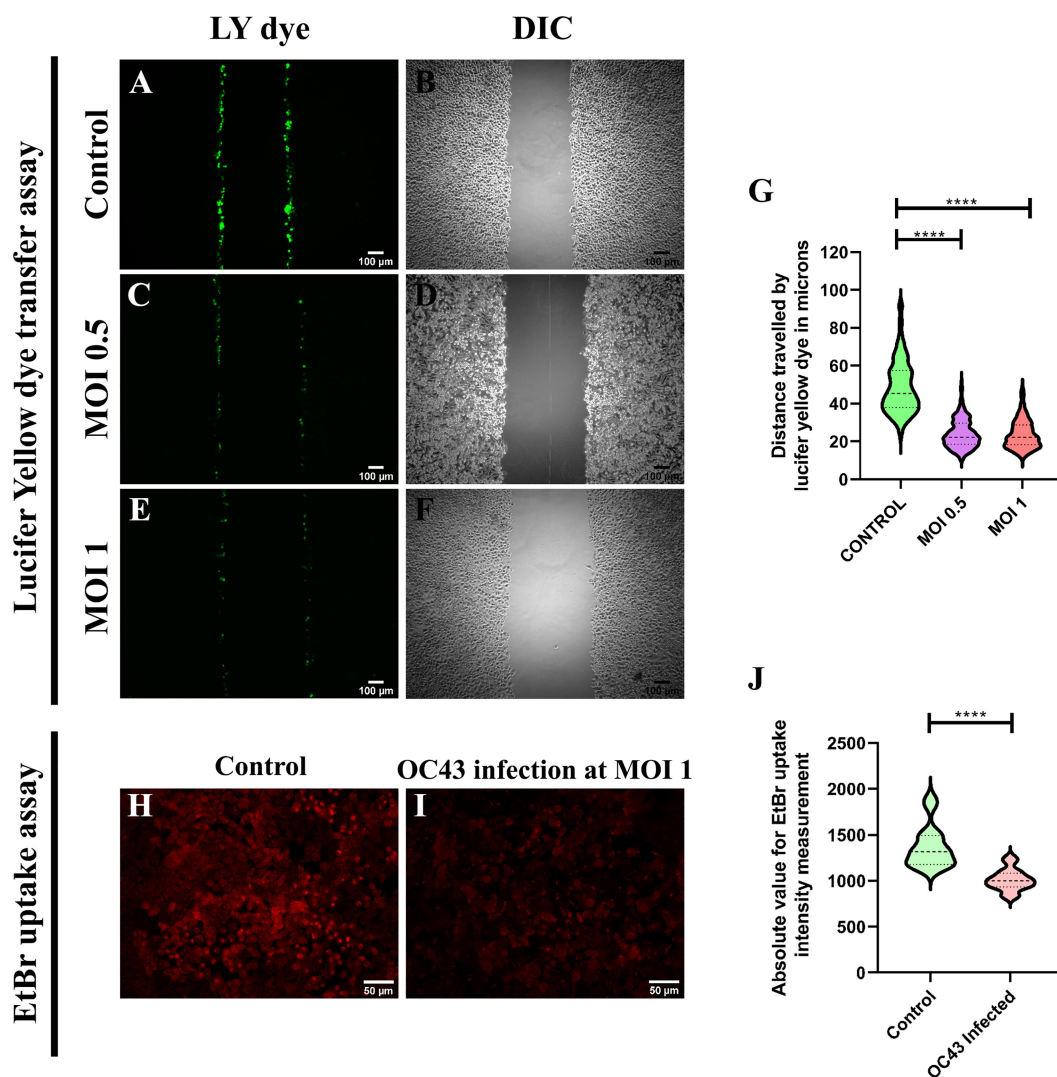
FIG 7 HCoV–OC43 impairs functional GJIC and hemichannel formation. For understanding the status of GJIC functionality, the LY dye was scrape-loaded in control (A) and MOIs 0.5 (C) and 1 (E) OC43-infected cells. It is observed that LY dye uptake and the distance traveled were less in infected A549 cells. Images B, D, and F are DIC images of the respective immunofluorescence fields. The distance traveled by the dye was quantified in ImageJ software, and absolute values were plotted in a violin plot (G). An EtBr uptake assay was performed with control and OC43-infected cells (H and I) to determine hemichannel activity. The absolute value for intensity was measured in ImageJ software and was plotted in a violin plot (J). The scale bar for the LY dye transfer assay images is 100 microns, and that for all the EtBr uptake assay images is 50 microns. Data are expressed as mean ± SEM of three individual replicates. The significant differences are indicated by *P < 0.05, **P < 0.01, ***P < 0.001, and ****P < 0.0001.

DISCUSSION

The recent pandemic caused by SARS-CoV-2, a member of the β-coronavirus genus, has left a lasting effect. Lack of research on the pathogenesis of human coronaviruses hindered the urgent need for therapeutics. Therefore, an enhanced understanding of the pathogenesis of human β-coronaviruses is crucial to improving our preparedness for combating future coronavirus infections. Given the high infectivity of SARS-CoV-2, another human β-coronavirus can be brought under consideration. OC43, also belonging to the β-coronavirus genus, primarily infects the upper respiratory tract and generally manifests a mild clinical condition of common cold (31). Given the close relationship between SARS-CoV-2 and OC43 within the β-coronavirus family, OC43 can serve as a valuable model for investigating the infection patterns of these human viruses.
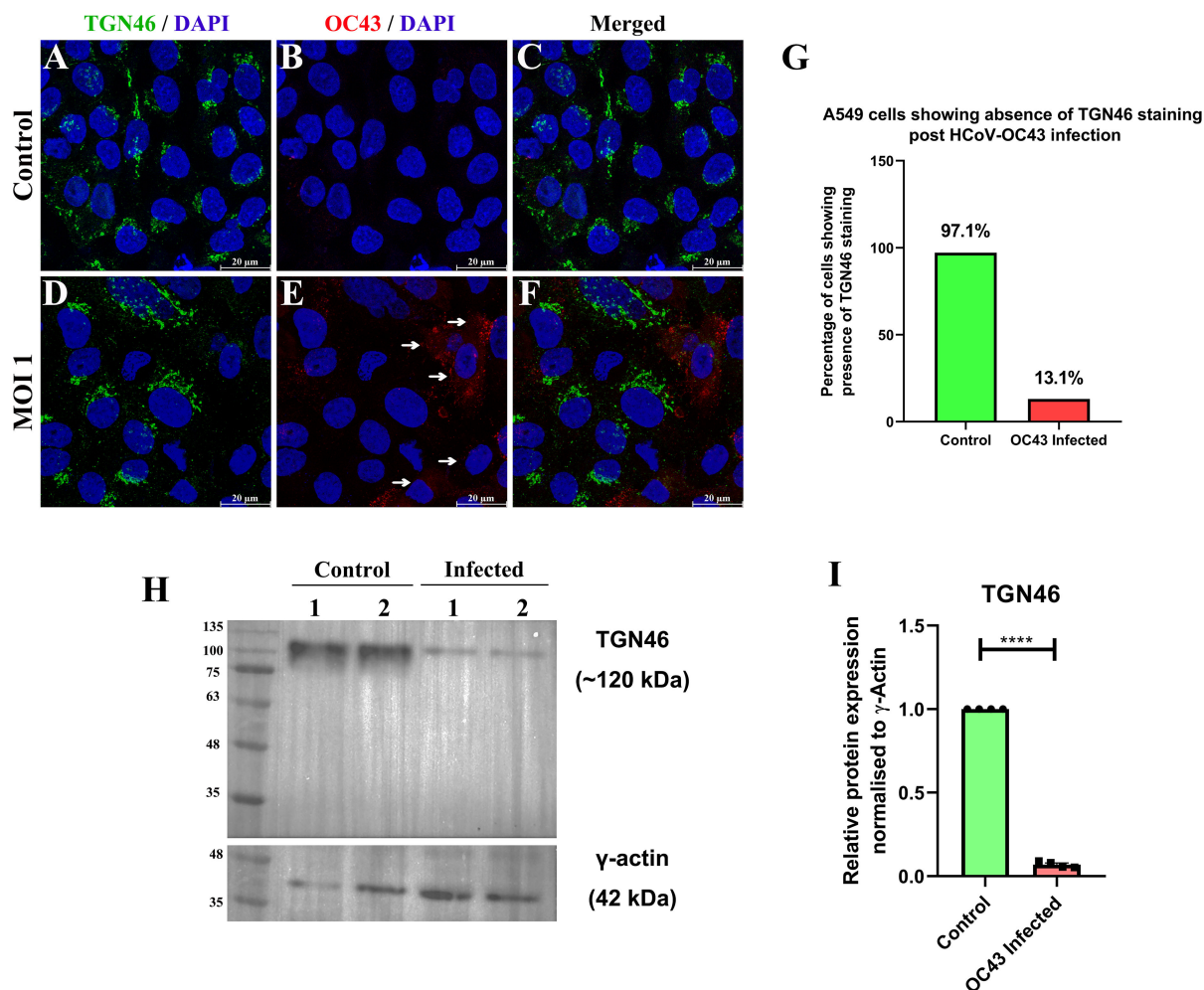
FIG 8 HCoV–OC43 infection disrupts the Golgi apparatus in A549 cells. To determine the mechanism of impaired Cx43-mediated GJIC, the status of the Golgi apparatus was studied through immunofluorescence staining and Western blot. Control and infected cells were stained with anti-TGN46 and anti-OC43 antibodies and counterstained with DAPI. Images A, B, and C represent control A549 cells, and images D, E, and F represent OC43-infected A549 cells. The white arrows depict infected cells either with complete loss of TGN46 staining or show disrupted TGN46 staining. The images were taken in a Leica SP8 confocal microscope. Images from the Olympus IX-81 microscope were analyzed, and the percentage of cells with the Golgi apparatus in both the control and infected cell populations was counted. A total of 500 cells were considered for each of the sets. The graph is shown in image G. To quantify the expression of TGN46 post-infection, 15 µg of the protein sample was loaded in each well, and Western blot analysis was performed, shown in image H. Scatterplot representing the densitometric analysis of TGN46 normalized with γ-actin is shown in image I. Control and infected lanes marked as 1 and 2, respectively, represent technical replicates. Data are expressed as mean ± SEM of two individual replicates. The significant differences are indicated by *$P < 0.05$, **$P < 0.01$, ***$P < 0.001$, and ****$P < 0.0001$. The scale bar for all the images is 20 microns.

This current study aimed to understand the role of human coronaviruses in modulating cell-to-cell communication by focusing on Cx43-mediated gap junction formation. Being expressed ubiquitously in a wide variety of cell lines and playing a crucial role in hemichannel formation, facilitating gap junction-mediated communication, Cx43 is an essential part of our study. To the best of our knowledge, this study is the first report showing an alteration in Cx43 expression and localization post-HCoV–OC43 infection. These changes directly affect cell-to-cell communication, essential for maintaining cellular homeostasis.

We demonstrated the ability of HCoV–OC43 to infect A549 cells and its infection transmission with respect to day points. With the help of this initial standardization, virus concentrations and incubation time were determined. As mentioned previously, Cx43-mediated cell-to-cell communication is an essential cellular process for maintaining cellular homeostasis. This study aims to understand the modulation of cell-to-cell
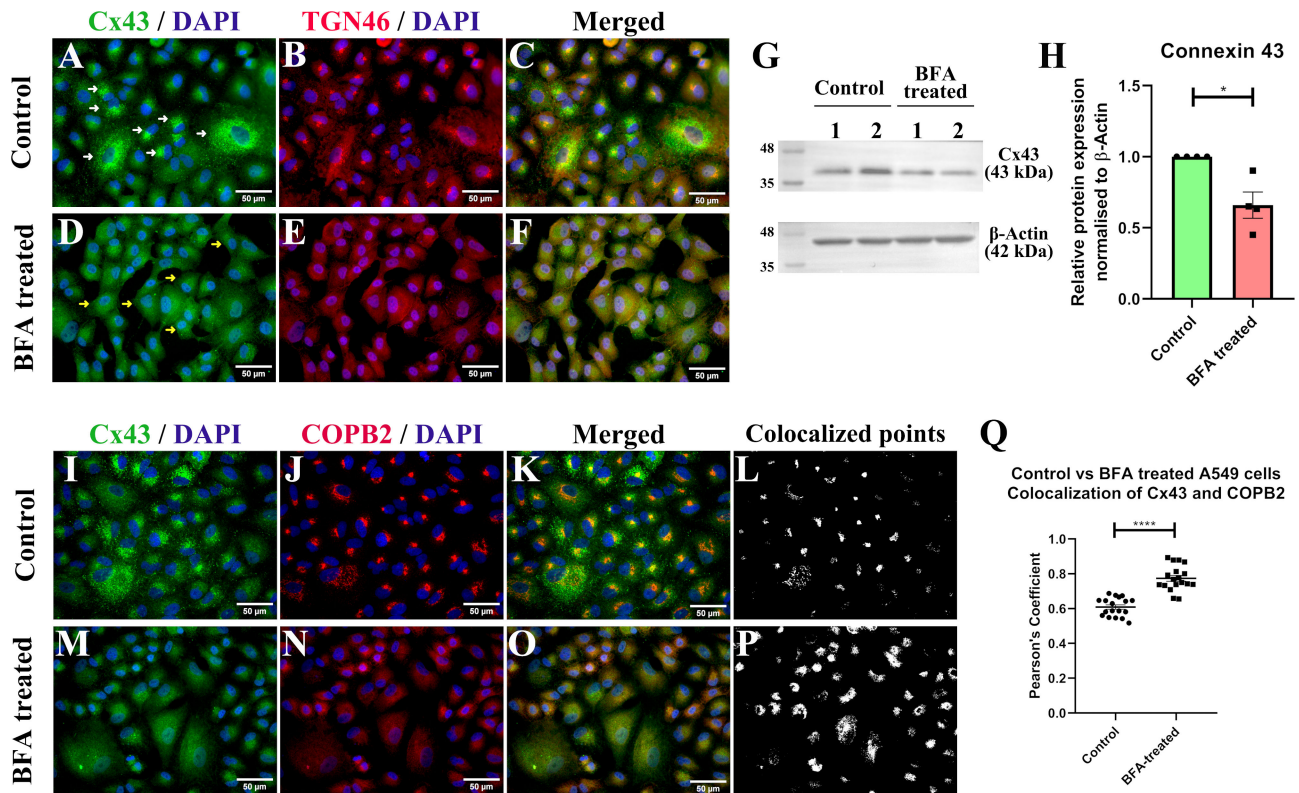
FIG 9 BFA treatment reduced Cx43 punctate staining and increased Cx43 localization with COPB2. To understand the effect of virus-induced Golgi apparatus disruption on Cx43 expression, A549 cells were treated with 0.2 µg/mL BFA for 24 hours. The cells were stained with anti-Cx43 and anti-TGN46 antibodies (A-F) and counterstained with DAPI. The control cells expressing punctate staining of Cx43 are marked with white arrows in image A. The BFA-treated cells showing reduced Cx43 punctate staining are shown with yellow arrows in image D. To quantify the decrease in Cx43 expression, Western blot analysis was performed using 15 µg of the protein sample loaded in each well (G). A scatterplot representing the densitometric analysis of Cx43 normalized with β-actin is shown in image H. To understand the localization of Cx43 post-Golgi apparatus disruption, the cells were treated with BFA and stained with anti-Cx43 and anti-COPB2 antibodies and counterstained with DAPI (I-P). The colocalized points of the control set are shown in image L and the BFA-treated cells in image P. Pearson's correlation coefficient values of colocalization are plotted in image Q as a scatterplot. The images are taken in the Olympus IX-81 microscope. Control and BFA-treated lanes marked as 1 and 2, respectively, represent technical replicates in image G. Data are expressed as mean ± SEM of two individual replicates. The significant differences are indicated by $*P < 0.05$, $**P < 0.01$, $***P < 0.001$, and $****P < 0.0001$. The scale bar for all the images is 50 microns.

communications through gap junctions in human β-coronavirus infection. Thus, targeting Cx43 in our research has provided insightful indications for developing therapeutic strategies. In our study, we have selected A549, which is a lung epithelial carcinoma cell line. The primary reason for choosing this cell line for our research is that the virus primarily infects the lungs. Also, the cell line considerably expresses Cx43 both in the cytosol and on the membrane. Therefore, A549 can serve as a good model for studying viral infectivity.

HCoV-OC43 infection in A549 cells revealed the downregulation of the gap junction protein Cx43 at the protein level. This was demonstrated with the help of immunoblot and immunofluorescence experiments. This alteration in the gap junction protein was accompanied by the increase of other stress markers such as ER stress indicated by HSP70, HSF1, and ERp29 and oxidative stress indicated by DJ-1. Heat shock factor 1 (HSF1) is critical in regulating cellular stress generated by unfolded proteins. Under normal conditions, HSF1 is present as monomers in the cytoplasm. Under stressful situations, HSF1 oligomerizes and is retained in the nucleus, where it binds to heat shock elements (HSE) of target genes. One such target gene is heat shock protein 70 (HSP70). HSP70 is a molecular chaperone expressed under stress, which binds to unfolded proteins and stabilizes them. Another ER-resident chaperone that regulates the synthesis and trafficking of several secretory and transmembrane proteins is ERp29. ERp29 is a

thioredoxin-homologous protein with various roles in ER stress and unfolded protein response (UPR). In several viral infections, including SARS-CoV-2, there is oxidative stress in the cells. DJ-1 is known to regulate oxidative stress. It has multiple functions, including antioxidant stress reaction and ROS scavenging (18). Immunoblot experiments confirmed the upregulation of these stress markers, which further indicates that the internalization of Cx43 may be responsible for increasing the overall stress factors of the cell. Upon infection with OC43, CX43 was observed to be localized in the perinuclear region in infected cells, mostly colocalizing with the ERGIC marker COPB2. The colocalization study was performed using the immunofluorescence staining technique, which helped understand the internal localization of Cx43. Triton X-100 solubilization assay confirmed the internal localization of Cx43 in infected cells as infected samples had less Triton X-100-insoluble GJIC plaques. However, we have performed the LY dye transfer assay and EtBr uptake assay to verify if this infectivity negatively regulates functional gap junction formation. The internalization of Cx43 results in alterations of functional gap junction and hemichannel formation, as confirmed by the LY dye transfer assay and EtBr uptake assay, respectively.

To understand the mechanism behind connexin 43 internalization and disruption during virus infection, we investigated if the Golgi apparatus has any role to play in this regard. In previous studies, it has been reported that different proteins of SARS-CoV-2 can disrupt the Golgi apparatus (32). To begin with, in the overall lifecycle of protein Cx43, it is first synthesized in the ER. It then exits the ER to the Golgi apparatus, and in the trans-Golgi, six connexin molecules bind to form a connexon, which is transported to the cell surface with the help of microtubules. Once connexons reach the cell surface, they form hemichannels or functional gap junction plaques (33). The Golgi apparatus plays a very important role in Cx43 protein assembly. Upon HCoV–OC43 infection, the trans-Golgi marker TGN46 protein expression is diminished in infected A549 cells. This affects Cx43 assembly and trafficking to the cell surface, and hence, Cx43 is retained within the perinuclear region in infected cells. Thus, it can be proposed that the mechanism for disruption of Cx43-mediated functional GJIC can be due to virus-induced Golgi fragmentation. To further confirm that Cx43 trafficking is impaired by virus-induced Golgi apparatus disruption, A549 cells were treated with BFA, a well-known Golgi-disrupting agent. BFA treatment showed similar characteristics when compared to an infected cell in terms of Cx43 protein expression. The punctate staining of Cx43 and overall Cx43 protein expression were observed to be significantly less in BFA-treated samples compared to non-treated samples. Finally, to determine the internal localization of Cx43, post-Golgi apparatus disruption, a colocalization study was performed between Cx43 and COPB2 in control and BFA-treated A549 cells. The colocalization of Cx43 and COPB2 in OC43-infected A549 cells was mirrored in BFA-treated A549 cells as well. This suggests a possible mechanism through which Cx43 protein expression and function are impaired by virus-induced Golgi apparatus disruption.

Previous studies from our lab have elucidated the alteration of Cx43 protein expression and localization in response to murine β-coronavirus infections. However, the studies to date were conducted using the mouse hepatitis virus (MHV) in glial cells. So we wanted to study the effect of a human virus, with its primary target site of infection being the lungs. This study would also provide insights into a pan-coronavirus infection model system. Thus, we selected OC43 as our model system in this study. Besides, MHV and OC43 differ in several aspects related to host infectivity, pathogenicity, and the pace of viral infectivity. MHV has been reported to primarily infect mice through carcinoembryonic antigen-related cell adhesion molecule 1 (CEACAM1) and is considered a model for studying acute and chronic-phase pathogenesis in mice. The pathogenicity of MHV can have various outcomes, from subclinical infections to severe diseases such as hepatitis, encephalitis, and respiratory distress, depending on the strain and host factors. MHV is known for its rapid replication kinetics in mice, leading to acute infections within short incubation periods. HCoV–OC43, on the other hand, infects humans through 9-O-acetylated sialic acid (9-O-Ac-Sia) and causes mild

respiratory symptoms resembling common cold. Sometimes, OC43 infection in young children, elderly, or immunocompromised individuals can even lead to more severe respiratory tract infections. OC43 infections in humans may have a slower onset, with an average incubation period of several days before the onset of the symptoms, but the extent of severity of symptoms varies depending on the immune response of the individual. The present study is conducted in a lung epithelial cell line as compared to the previous studies with MHV, which were conducted on glial cells. The primary site of infection of β-coronavirus is the lungs, so A549 was chosen as the cell line to study the effect of a human β-coronavirus infection on gap junction-mediated cell-to-cell communication. Similar results were obtained in previous studies compared to those of the current study, with respect to reduced Cx43 expression, impairment of functional GJIC, and increase in ER stress, but with downregulation in Erp29 protein expression. HCoV–OC43 infection in A549 cells showed an increase in Erp29 protein expression and also revealed the disruption of the Golgi apparatus, which might be directly linked to Cx43 protein expression and trafficking. Hence, the current study holds importance in expanding our knowledge in the area of changes in Cx43-mediated functional GJIC post-human β-coronavirus infection. These studies in murine β-coronavirus MHV and HCoV–OC43 offer insights into the modulation of cell-to-cell communication post-infection in a pan-coronavirus infection model system.

Our research has unveiled the pivotal role of viral infections in remodeling intercellular communication. It is clear that intercellular communication is essential for cellular homeostasis. Indeed, previous studies from our lab have reported that treatment with a chemical chaperone 4-phenylbutyric acid (4-PBA) showed an increased capacity of Cx43 to traffic to the cell surface and can form functional gap junction channels. 4-PBA treatment attenuated the harmful effects of MHV infection, such as ER stress and reduced Cx43 protein expression(10), thus providing insights into reduced virus infection upon increased Cx43 protein expression and trafficking. Since OC43 is a relatively new model system, it provides good implications for developing therapeutic targets for human coronaviruses by finely regulating the expression of Cx43.

AUTHOR AFFILIATION

[1]Department of Biological Sciences, Indian Institute of Science Education and Research Kolkata, Mohanpur, India

AUTHOR ORCIDs

Souvik Karmakar http://orcid.org/0009-0003-1529-4996
Jayasri Das Sarma http://orcid.org/0000-0002-3980-4060

AUTHOR CONTRIBUTIONS

Souvik Karmakar, Conceptualization, Data curation, Formal analysis, Investigation, Methodology, Software, Writing – original draft, Writing – review and editing | Jayasri Das Sarma, Conceptualization, Funding acquisition, Investigation, Project administration, Resources, Supervision, Validation, Visualization, Writing – review and editing

DATA AVAILABILITY

The data are available within this article or from the authors upon request.

REFERENCES

1. Weber PA, Chang HC, Spaeth KE, Nitsche JM, Nicholson BJ. 2004. The permeability of gap junction channels to probes of different size is dependent on connexin composition and permeant-pore affinities. Biophys J 87:958–973. https://doi.org/10.1529/biophysj.103.036350

2. Goodenough DA, Paul DL. 2009. Gap junctions. Cold Spring Harb Perspect Biol 1:a002576. https://doi.org/10.1101/cshperspect.a002576

3. Li MWM, Mruk DD, Lee WM, Cheng CY. 2010. Connexin 43 is critical to maintain the homeostasis of the blood-testis barrier via its effects on tight junction reassembly. Proc Natl Acad Sci U S A 107:17998–18003. https://doi.org/10.1073/pnas.1007047107

4. Li S, Armstrong N, Zhao H, Cruz-cosme R, Yang H, Zhong C, Fu W, Wang W, Yang D, Xia N, Cheng T, Tang Q. 2022. Zika virus infection downregulates connexin 43, disrupts the cardiomyocyte gap junctions and induces heart diseases in A129 mice. J Virol 96:1–18. https://doi.org/10.1128/jvi.01373-22

5. Khan Z, Yaiw K-C, Wilhelmi V, Lam H, Rahbar A, Stragliotto G, Söderberg-Nauclér C. 2014. Human cytomegalovirus immediate early proteins promote degradation of connexin 43 and disrupt gap junction communication: Implications for a role in gliomagenesis. Carcinogenesis 35:145–154. https://doi.org/10.1093/carcin/bgt292

6. Calhoun PJ, Phan AV, Taylor JD, James CC, Padget RL, Zeitz MJ, Smyth JW. 2020. Adenovirus targets transcriptional and posttranslational mechanisms to limit gap junction function. FASEB J. 34:9694–9712. https://doi.org/10.1096/fj.202000667R

7. Basu R, Banerjee K, Bose A, Das Sarma J. 2016. Mouse hepatitis virus infection remodels connexin43-mediated gap junction intercellular communication in vitro and in vivo . J Virol 90:2586–2599. https://doi.org/10.1128/JVI.02420-15

8. Basu Rahul, Bose A, Thomas D, Das Sarma J. 2017. Microtubule-assisted altered trafficking of astrocytic gap junction protein connexin 43 is associated with depletion of connexin 47 during mouse hepatitis virus infection. J Biol Chem 292:14747–14763. https://doi.org/10.1074/jbc.M117.786491

9. Bose A, Basu R, Maulik M, Das Sarma J. 2018. Loss of Cx43-mediated functional gap junction communication in meningeal fibroblasts following Mouse hepatitis virus infection. Mol Neurobiol 55:6558–6571. https://doi.org/10.1007/s12035-017-0861-3

10. Bose A, Kasle G, Jana R, Maulik M, Thomas D, Mulchandani V, Mukherjee P, Koval M, Das Sarma J. 2023. Regulatory role of endoplasmic reticulum resident chaperone protein ERp29 in anti-murine β-coronavirus host cell response. J Biol Chem 299:102836. https://doi.org/10.1016/j.jbc.2022.102836

11. Giepmans BNG, Moolenaar WH. 1998. The gap junction protein connexin43 interacts with the second PDZ domain of the zona occludens-1 protein. Curr Biol 8:931–934. https://doi.org/10.1016/s0960-9822(07)00375-2

12. Burchfiel ET, Vihervaara A, Guertin MJ, Gomez-Pastor R, Thiele DJ. 2021. Comparative Interactomes of HSF1 in stress and disease reveal a role for CTCF in HSF1-mediated gene regulation. J Biol Chem 296:100097. https://doi.org/10.1074/jbc.RA120.015452

13. Evans CG, Chang L, Gestwicki JE. 2010. Heat shock protein 70 (Hsp70) as an emerging drug target introduction to Hsp70 structure and function. Journal of Medicine chemistry 53:4585–4602. https://doi.org/10.1021/jm100054f

14. Mayer MP, Bukau B. 2005. Hsp70 chaperones: cellular functions and molecular mechanism. Cell Mol Life Sci 62:670–684. https://doi.org/10.1007/s00018-004-4464-6

15. Das S, Smith TD, Sarma JD, Ritzenthaler JD, Maza J, Kaplan BE, Cunningham LA, Suaud L, Hubbard MJ, Rubenstein RC, Koval M. 2009. ERp29 restricts connexin43 oligomerization in the endoplasmic reticulum. Mol Biol Cell 20:2593–2604. https://doi.org/10.1091/mbc.e08-07-0790

16. Brecker M, Khakhina S, Schubert TJ, Thompson Z, Rubenstein RC. 2020. The probable, possible, and novel functions of ERp29. Front Physiol 11:574339. https://doi.org/10.3389/fphys.2020.574339

17. Ariga H, Takahashi-Niki K, Kato I, Maita H, Niki T, Iguchi-Ariga SMM. 2013. Neuroprotective function of dj-1 in Parkinson's disease. Oxid Med Cell Longev 2013:683920. https://doi.org/10.1155/2013/683920

18. Zhang L, Wang J, Wang J, Yang B, He Q, Weng Q. 2020. Role of Dj-1 in immune and inflammatory diseases. Front. Immunol 11:1–10. https://doi.org/10.3389/fimmu.2020.00994

19. Arbour N, Côté G, Lachance C, Tardieu M, Cashman NR, Talbot PJ. 1999. Acute and persistent infection of human neural cell lines by human coronavirus OC43. J Virol 73:3338–3350. https://doi.org/10.1128/JVI.73.4.3338-3350.1999

20. Jacomy H, Talbot PJ. 2006. HCoV-OC43-induced apoptosis of murine neuronal cells. Adv Exp Med Biol 581:473–478. https://doi.org/10.1007/978-0-387-33012-9_84

21. Lambert F, Jacomy H, Marceau G, Talbot PJ. 2008. SARS- and other Coronaviruses. In Cavanagh D, Totowa NJ (ed), Methods in molecular biology. Vol. 454. Humana Press.

22. Favreau DJ, Desforges M, St-Jean JR, Talbot PJ. 2009. A human coronavirus OC43 variant harboring persistence-associated mutations in the S glycoprotein differentially induces the unfolded protein response in human neurons as compared to wild-type virus. Virology 395:255–267. https://doi.org/10.1016/j.virol.2009.09.026

23. St-Jean JR, Jacomy H, Desforges M, Vabret A, Freymuth F, Talbot PJ. 2004. Human respiratory coronavirus OC43: genetic stability and neuroinvasion. J Virol 78:8824–8834. https://doi.org/10.1128/JVI.78.16.8824-8834.2004

24. Lei C, Yang J, Hu J, Sun X. 2021. On the calculation of TCID50 for quantitation of virus infectivity. Virol. Sin 36:141–144. https://doi.org/10.1007/s12250-020-00230-5

25. Dallner M, Harlow J, Nasheri N. 2021. Human coronaviruses do not transfer efficiently between surfaces in the absence of organic materials. Viruses 13:1352. https://doi.org/10.3390/v13071352

26. Schneider CA, Rasband WS, Eliceiri KW. 2012. NIH image to imageJ: 25 years of image analysis. Nat Methods 9:671–675. https://doi.org/10.1038/nmeth.2089

27. Mulchandani V, Banerjee A, Vadlamannati AV, Kumar S, Das Sarma J. 2023. Connexin 43 trafficking and regulation of gap junctional intercellular communication alters ovarian cancer cell migration and tumorigenesis. Biomedicine & Pharmacotherapy 159:114296. https://doi.org/10.1016/j.biopha.2023.114296

28. Sadasivan J, Singh M, Sarma JD. 2017. Cytoplasmic tail of coronavirus spike protein has intracellular targeting signals. J Biosci 42:231–244. https://doi.org/10.1007/s12038-017-9676-7

29. Nielsen MS, Axelsen LN, Sorgen PL, Verma V, Delmar M, Holstein-Rathlou N-H. 2012. Gap junctions, p 1981–2035. In Compr physiol. Wiley.

30. Nollevaux G, Devillé C, El Moualij B, Zorzi W, Deloyer P, Schneider Y-J, Peulen O, Dandrifosse G. 2006. Development of a serum-free co-culture of human intestinal epithelium cell-lines (Caco-2/HT29-5M21). BMC Cell Biol 7:20. https://doi.org/10.1186/1471-2121-7-20

31. Liu DX, Liang JQ, Fung FT. 2021. Human coronavirus-229E, -OC43, -NI63, and -HKU1 (Coronaviridae), p 428–440. In Encyclopedia of virology. Elsevier.

32. Hackstadt T, Chiramel AI, Hoyt FH, Williamson BN, Dooley CA, Beare PA, de Wit E, Best SM, Fischer ER. 2021. Disruption of the golgi apparatus and contribution of the endoplasmic reticulum to the sars-cov-2 replication complex. Viruses 13:1798. https://doi.org/10.3390/v13091798

33. Segretain D, Falk MM. 2004. Regulation of connexin biosynthesis, assembly, gap junction formation, and removal. Biochim Biophys Acta Biomembr 1662:3–21. https://doi.org/10.1016/j.bbamem.2004.01.007